

## P14.6 CORRELATION OF LIGHTNING FLASH RATES WITH A MICROBURST EVENT

Karen M. Altino\* and Kevin R. Knupp  
University of Alabama in Huntsville, Huntsville, Alabama

Steven J. Goodman  
Earth Science Dept., NASA/Marshall Space Flight Center, Huntsville, Alabama

### 1. INTRODUCTION

In 1986 the MIST (Microburst and Severe Thunderstorm) field study took place over northern Alabama (Atkins and Wakimoto 1991). It was noted that the time of day when a peak in microburst activity was observed usually took place around 2000 UTC. It was further confirmed through the examination of the various PAM (Portable Automated Mesonet) stations that this was also the time of day where temperatures would reach their peak. On the afternoon of 18 August 2002, as the temperature approached a daily high temperature of 32 °C, the first radar indication of the HSV microburst-producing storm initiated at 2020 UTC.

By the time the Huntsville storm (hereafter referred to as the HSV storm) had deteriorated, it had produced hail and strong winds. Widespread lightning damage occurred as the storm produced flash rates not often observed in non-supercell systems. The HSV storm began at 2023 UTC and, for a 5-minute radar scan beginning at 2116 UTC, the North Alabama National Lightning Detection Network (NLDN) data indicated a peak CG lightning rate of 8.6 flashes/min. At this same time, the NASA Lightning Mapping Array (LMA) network recorded a total flash rate of 4.43 flashes/second. The microburst event occurred at 2117 UTC with a recorded wind gust exceeding 34 m s<sup>-1</sup>. At 2126 UTC, the NWS issued a severe thunderstorm warning for Madison County. At this same time, the LMA network recorded 1769 total flashes over the next five minutes – a rate of 5.9 flashes *per second*. Additionally, at 2130 UTC, 19 mm diameter hail was reported in southwest Huntsville near the city of Madison. Finally, a flash flood warning was issued for Madison County at 2151 UTC as some areas received more than 100 mm of rain over the two-hour time span.

### 2. METHODOLOGY

#### 2.1 Data Sources

Radar measurements were obtained from the National Weather Service's WSR-88D Doppler radar (KHTX) located in Hytop, Alabama. The NLDN collected CG lightning data while total lightning information was achieved by the LMA network; both systems are located in northern Alabama. Surface observations were obtained from the following locations:

- the FAA Automated Surface Observing Systems (ASOS) located in Huntsville and Decatur, Alabama

- the National Space Science and Technology Center (NSSTC) weather station, located on the campus of the University of Alabama in Huntsville (UAH)
- Redstone Technical Test Center's Surface Automated Mesonet Station (SAMS) located on Redstone Arsenal in Huntsville.

Fig. 1 indicates the location of each of the above-mentioned instruments in relation to the city of Huntsville.

Visible and infrared imagery was obtained from the NASA GOES-8 orbiting satellite. This information was used to examine thunderstorm cloud fields and identify possible boundaries within the region that may have assisted rapid storm intensification. The Cooperative Huntsville-Area Rainfall Measurements (CHARM) Network compiled other 24-hour totals for the region.

#### 2.2 Data Processing Methodology

##### 2.2.1 Upper air soundings

Upper air sounding data from Nashville, Tennessee (BNA) and Birmingham, Alabama (BMX) were also collected for 18 August 2002 (1200 UTC) and 19 August 2002 (0000 UTC). A composite sounding generated for the Huntsville area was created to provide an estimate of environmental conditions at 2000 UTC – approximately 20 minutes before the first radar echo and a little more than an hour before the microburst

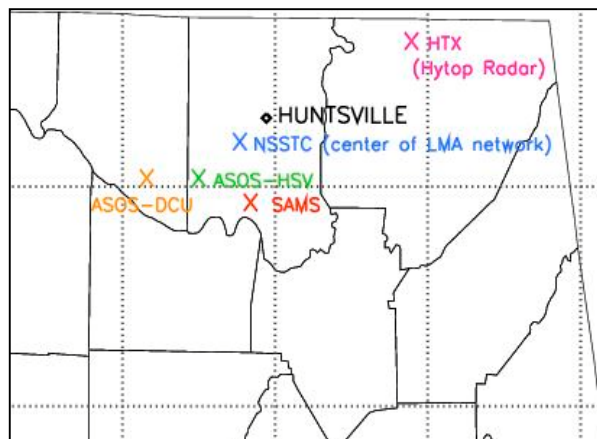


FIG. 1. Map of northern Alabama. The city of Huntsville is located in Madison County along with the NSSTC, SAMS, and ASOS-HSV instruments. The ASOS-DCU observation system is located in Limestone County, while the Hytop radar (HTX) resides in Jackson County.

\* Corresponding author address: Karen Altino, Univ. of Alabama in Huntsville (UAH), National Space Science and Technology Center (NSSTC), Huntsville, AL 35805; email: [karen.altino@nsstc.uah.edu](mailto:karen.altino@nsstc.uah.edu)

event. The Nashville sounding at 0000 UTC most likely resembled environmental conditions of the storm. Neither the 1200 UTC BNA sounding nor any of the BMX soundings indicated a boundary in place more than 7 hours prior to storm initiation.

The BNA site is approximately 180 km north of Huntsville (see Fig. 2). The 0000 UTC BNA sounding was modified by replacing the surface temperature ( $T$ ) and dewpoint ( $T_d$ ) on the BNA 0000 UTC sounding using surface  $T$  and  $T_d$  readings from the ASOS-HSV station when these storms fired up along the boundary late that afternoon.

### 2.2.2 NWS WSR-88D Doppler radar

Level II Doppler radar data acquired from the KHTX radar was viewed with the National Center for Atmospheric Research (NCAR) SOLO editing software. Storm motion and growth was analyzed using this software and storm focus was determined after reviewing reflectivity and velocity patterns of both the Huntsville microburst-producing storm (hereafter referred to as the HSV storm) and other surrounding strong storms. The NCAR REORDER software was then used to transform the radar data into Cartesian coordinates. For the HSV storm, the Cressman weighting function was applied and a radius of influence of 1 km in the x- and y-directions, 1.5 in the z-direction were used, and a grid spacing of .5 km was utilized for this case.

Once the radar data was translated into Cartesian space, NCAR's Custom Editing and Display of Reduced Information in Cartesian Space (CEDRIC) software was used to contour the data and create horizontal CAPPIs and reconstructed vertical RHLs of the storms being reviewed. CEDRIC was also used to create three-dimensional reflectivity contours and to calculate the vertically integrated water (VIL) for the HSV storm. VIL was calculated using the Z-M relationship as described by Greene and Clark (1972). The value for liquid water content ( $M$ ) was calculated from reflectivity factor ( $Z$ ) using

$$M = 3.44 \times 10^{-3} Z^{4/7} \quad (1)$$

where the units for  $M$  are  $\text{gm m}^{-3}$  and the units for  $Z$  are  $\text{mm}^6 \text{m}^{-3}$ .  $M$  was then integrated over all height levels to achieve  $M^*$  – the vertically integrated liquid water (VIL) value,

$$M^* = 3.44 \times 10^{-3} \int_{h_{\text{base}}}^{h_{\text{top}}} Z^{4/7} dh' \quad (2)$$

where  $h'$  is the height in meters and the units for  $M^*$  are  $\text{kg m}^{-2}$ .

### 2.2.3 GOES-8 satellite imagery

The Global Hydrology and Climate Center (GHCC), located within the NSSTC, operates two NASA Geostationary Operational Environmental Satellite (GOES) ground stations on the roof of the NSSTC – one for GOES-8 (since upgraded to GOES-12) and one for

GOES-10. From this, GOES-8 visible and infrared imagery is retrieved for the southeast region of the U.S. For the infrared satellite images, the resolution is always 4 km. Visible images, however, change every fifteen minutes – on the half-hour it provides a 1-km spatial resolution while at 15-min and 45-min past the hour the resolution is 4 km. GOES-8 images from 90 minutes prior to the HSV storm's microburst event were examined. However, the last image from the NSSTC antennas came at 2045 UTC as the intensity of the developing cell's winds shifted the antennas off by a few degrees, causing the instruments to go offline until 0115 UTC on 19 August 2002 – well past the severe storm event. The GOES-8 imagery prior to the storm was useful in that it further defined the boundary in the region and its pre-storm images will be presented later in this paper.

### 2.2.4 Surface station data

Surface data for ASOS and the NSSTC weather station were recorded every minute, while SAMS sampled 15-min averages every fifteen minutes. Surface station data from all stations was conformed to standard units. Plots for wind speed, wind direction, temperature, dewpoint, and rainfall were generated for each site. Both SAMS and the NSSTC anemometer provided peak wind information as well from their sites.

The CHARM network was established in 2001 and its data comes from both organizations and individuals that have volunteered to collect and report daily rainfall amounts at their locations. For this case study, rainfall reports clearly showed the areas where extreme localized flooding occurred during the two-hour HSV storm event.

### 2.2.5 Lightning detection methods

The NLDN has over 100 ground-based remote sensors throughout the United States, including 59 Lightning Position and Tracking System (LPATS) sensors. One of these LPATS sensors resides in northern Alabama. Each sensor is based on time-of-arrival (TOA) information.

For this study, the detected NLDN CG strokes for each storm were determined by calculating the total number of CG strokes within a  $0.2^\circ \times 0.2^\circ$  box around the center of the storm. [The storm centers were determined to be where the highest reflectivity values occurred for each radar volume scan.] The flashes were separated into negative and positive flashes, and comparisons will be presented in a later section. All CG flashes were taken into account; flashes in excess of 10 kA were included in this particular study due to the intense flash rates. Noise or interference from strong IC lightning may have contributed to these higher current readings, but LMA data infers that these are probably legitimate flashes. As this study is still ongoing, the understanding of these values and their accuracy is still being examined.

The North Alabama LMA network is composed of an array of ten VHF sensors scattered within a 50 km

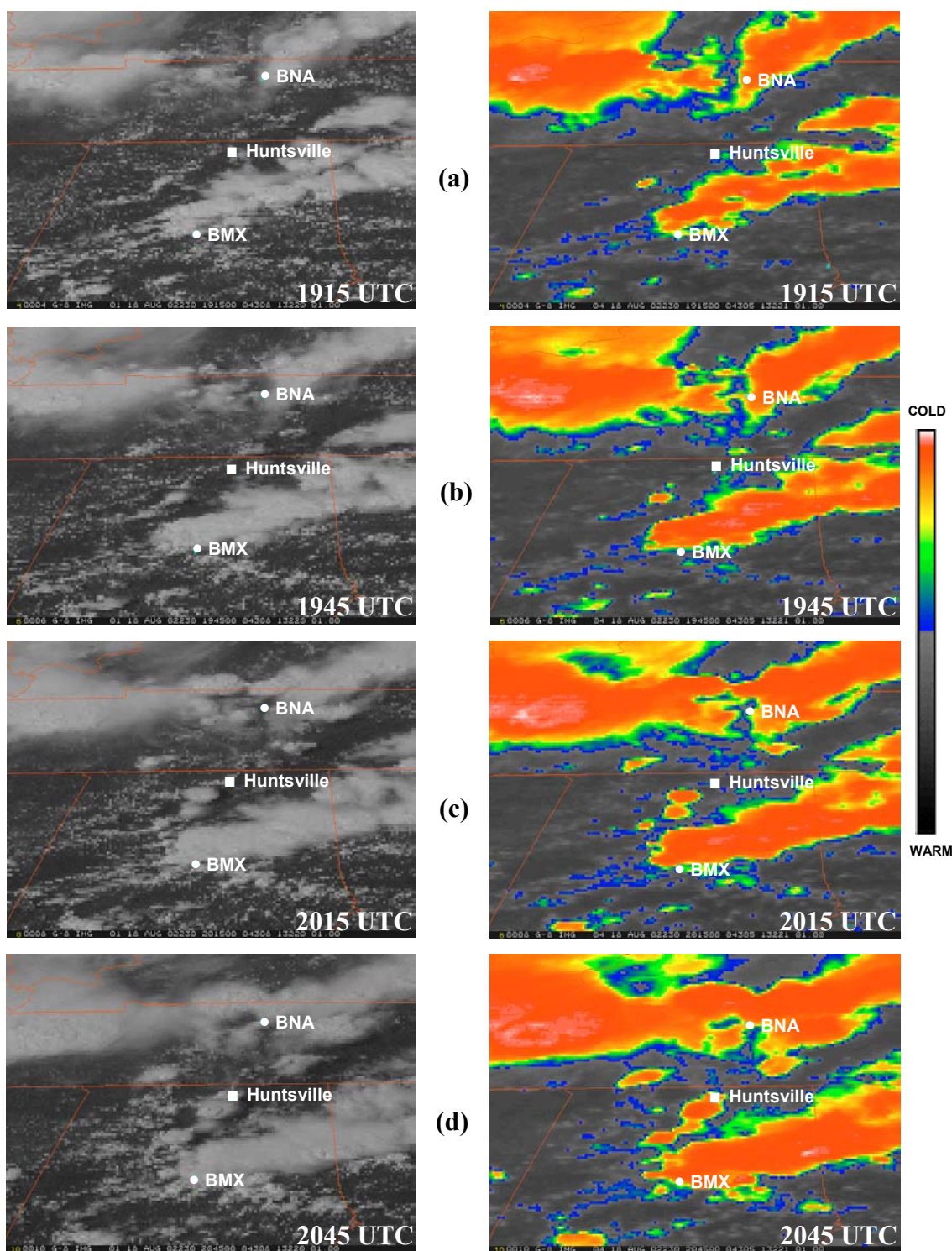


FIG. 2. GOES-8 4-km resolution visible (left) and infrared (right) images. The locations of the city of Huntsville as well as the launch sites of the BMX and BNA soundings have been superimposed. (a) At 1915 UTC Huntsville lies along the boundary. (b) A second storm to the SW of Huntsville is strengthening. (c) The HSV storm cloud tops begin to grow. (d) The cloud tops begin to quickly rise and cool, creating the initial anvil of the storm.

radius of Huntsville. Of the ten sensors, four are relay sites with a base station located at the NSSTC (Blakeslee 2004). The LMA network runs on a 72-78 MHz bandwidth (channel 5) and has a minimal detectable signal of 0.1 watts. These antennas also independently detect the VHF radio waves emitted from lightning and use a TOA method of measurement. The LMA has an efficiency radius of 150 km (Rison 2004). Past this distance, the efficiency drops off as the ability to distinguish between valid sources and noise becomes an issue.

It can be difficult to determine which sources go to which flash. With storm cells developing near one another, both the NLDN and LMA networks have room for errors as sources/flashes from other storms may affect and/or influence the rates of an individual storm. One advantage of the HSV storm was, prior to the mergers, no other storms were close enough to influence the data. In examining the LMA data, the same type of  $0.2^\circ \times 0.2^\circ$  box around the storm core was examined in the same manner as for the NLDN data. After receiving the LMA in hourly data files, the data was broken up into times matching the radar scan times.

The built-in flash algorithm contained within New Mexico Tech's XLMA program was used to determine the total number of flashes within the North Alabama region, including the NLDN flashes. This algorithm identifies, divides, and groups data from the LMA into flashes and flash types. It is assumed that all sources within the same time and space belong to a single flash (Thomas et al. 2003). There are restrictions on how large the gap for both these variables can be, but the usual criteria requires the sources to be located within 3 km of each other and no more than 150 ms apart. As this storm was highly electrified, some errors in data separation may have occurred but the more important lightning trends would remain in tact and it is these trends that become important in understanding the nature of this storm.

### 3.1 Satellite Imagery

Approximately five hours prior to the HSV storm, a rain event with wind speeds  $\leq 3.6 \text{ m s}^{-1}$  and a total rainfall amount of 2.03 mm (as recorded by the NSSTC) occurred between 1643 – 1730 UTC that morning over the Huntsville region. In effect, the event left behind a region of cool surface air and an associated boundary for storms to form along during the late afternoon hours. Fig. 2 shows a series of GOES-8 images – visible on the left, infrared on the right – from approximately one hour prior to the first radar indication of the storm until about 30 minutes before the microburst event. After this, the NSSTC antennas were shifted off-course by high winds and rain and remained offline until 0115 UTC on 19 August. All images have a 4-km resolution.

The GOES-8 visible and infrared images at 1915 UTC in Fig. 2 clearly indicate the boundary, shown by the thin cumulus cloud line extending from west central Alabama (near the Mississippi border) cutting northeast through Birmingham (where it appears to be cloudy) and up through north central Alabama (near the Tennessee

border). At 1915 UTC, the cold cloud tops are located in northwest Tennessee and south to east of Huntsville but it is clear that storms are beginning to form along this line near Huntsville. By 2015 UTC, the cold cloud tops of the HSV storm emerge in the images as the storm begins to intensify.

### 3.2 Surface Station Data

Data sets from ASOS-HSV, SAMS, and the NSSTC were closely examined. The temperature data from each station is shown in Fig. 3. At the NSSTC – where the most intense portion of the storm occurred – recorded its daily high prior to the storm but saw a second rise in temperature not long after the storm began to form. This lasted for about 5 minutes before a rapid drop in temperatures occurred – a drop-off of more than  $6^\circ \text{C}$  over a 10-min time span indicating the cool side of the boundary. The ASOS-HSV system recorded a daily high at about the same time the HSV storm initiated. This is indicative of the warm side of the boundary. SAMS saw a small drop in temperature just before and during the microburst, but the temperature then resumed increasing over time.

### 3.3 Upper Air Soundings

The soundings for Nashville (BNA) and Birmingham (BMX) at 1200 UTC on 18 August showed two different environments. The BMX sounding showed a fairly stable atmosphere, with a CAPE value of  $466 \text{ J kg}^{-1}$  and pocket of dry air just above the surface. The BNA sounding indicated a CAPE value of  $1930 \text{ J kg}^{-1}$  and a very moist layer of air extending up to 950 mb. However, both these soundings indicated what the upper air conditions were prior to the mid-morning storms that set up the boundary – about 8 hours prior to the afternoon storm initializations. The BNA 0000 UTC sounding for 19 August was reviewed and used to create a modified sounding for Huntsville.

One thing that was not changed from the original

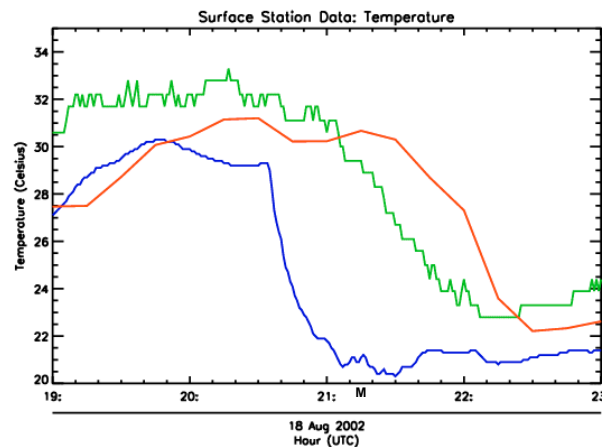


FIG. 3. Image of temperature readings from the ASOS-HSV, NSSTC, and SAMS instruments for 1900-2300 UTC on 18 August 2002. "M" indicates the time of the microburst event at 2117 UTC as recorded by the NSSTC anemometer.

sounding was the wind data. The BNA sounding indicated light winds at the surface and weak vertical shear aloft. This indication of a low shear environment was in place as the boundary moved through and the storms began initiating.

The boundary that remained in place over the region extended from southwest to northeast (as seen in Fig. 2). Storms were still forming and evolving along this boundary in the south central Tennessee region hours after the storms ceased in the Huntsville area. The 0000 UTC BNA sounding was modified by replacing the BNA readings of  $T=26.8^{\circ}\text{C}$  and  $T_d=21.9^{\circ}\text{C}$  with the ASOS-HSV readings of  $T=32.2^{\circ}\text{C}$  and  $T_d=23.3^{\circ}\text{C}$  taken from 2000 UTC. The modified sounding has a CAPE value of  $\sim 4200 \text{ J kg}^{-1}$  (Fig. 4).

## 4. STORM CHARACTERISTICS

### 4.1 Rainfall

Rainfall amounts varied greatly over the Huntsville region. The ASOS station in western Madison County recorded a total of 8.83 mm of rain, while the SAMS station south of the NSSTC recorded no rainfall at all. In stark contrast, the NSSTC surface station recorded 101.6 mm of rain as the storm occurred directly over the site. Fig. 5 shows rainfall amounts as recorded by the CHARM network. The location of heavy rainfall

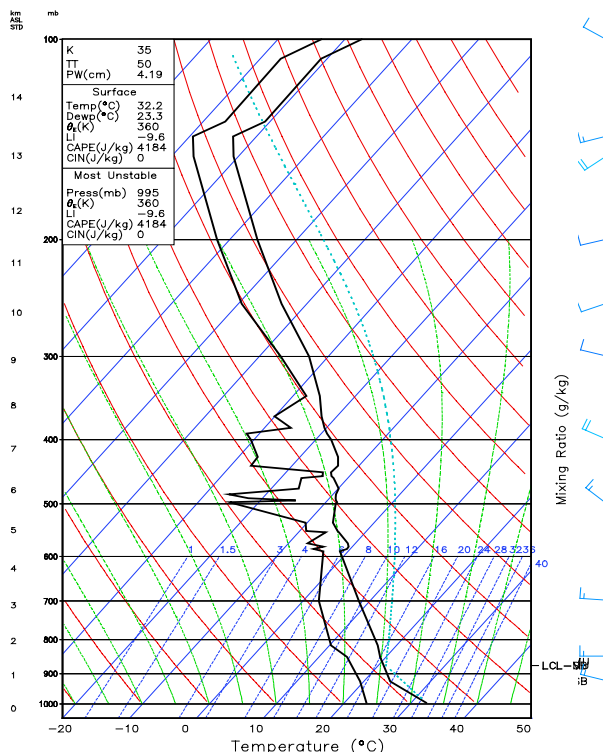


FIG. 4. Modified sounding for the Huntsville region. This sounding is based on the 19 August 0000 UTC sounding out of Nashville (BNA). This sounding was created by replacing the surface  $T$  and  $T_d$  with those from the ASOS-HSV station at 2000 UTC on 18 August 2002. Though somewhat exaggerated, possible CAPE values could have been over  $4000 \text{ J kg}^{-1}$  at the time of the HSV storm.

### CHARM Network Rainfall Totals for 18 August 2002

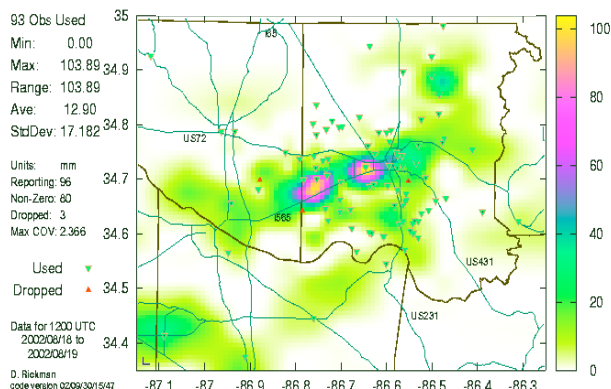


FIG. 5. CHARM rainfall map for 18 August 2002. There were two maximums on this date. The first occurred directly over southwest Huntsville, near the NSSTC and the surrounding area. The second maximum occurred out toward the city of Madison. This area also saw small hail with this storm, but they did not encounter the same intense winds.

amounts agrees with the data provided by the previously mentioned instruments. An area of excessive rainfall fell within an approximately 5-km radius around the NSSTC. Streets in this area quickly became flooded and a flash flood warning for Madison County was issued by the NWS at 2151 UTC.

### 4.2 Lightning Densities

Fig. 6 shows a log density map produced with preliminary data for the HSV storm. This image was produced using the New Mexico Tech XLMA software. Even though the number of points was later found to be much higher than this initial count, the main point of interest is the intense density of lightning sources that occurred over the Huntsville area. There is a second area to the SSW of HSV that contained a high density of sources as well, though not nearly as many as the HSV storm. Ongoing studies indicate that this occurred when a strong storm – which contained hail and produced a higher reflectivity at the ground – merged with a smaller storm.

### 4.3 Storm Motion and Reflectivity

One of the characteristics that made the HSV storm stand out from most storms that occurred this day was the storm's anomalous motion. Though it averaged a horizontal motion of approximately  $3 \text{ m s}^{-1}$  over its lifetime, the motion prior to the microburst averaged less than  $1 \text{ m s}^{-1}$ . Other storms in the area moved to the ESE at an average rate  $\geq 5 \text{ m s}^{-1}$ . Following the area of highest reflectivity, the core of the HSV storm slowly moved east before it started drifting WSW. Not only did this cause localized flooding but it also allowed the opportunity for other storms to interact with it. As a result, a few smaller storms merged with the HSV storm at various stages of its lifecycle and, therefore, it was difficult to isolate the reflectivity for this storm and follow it through the end stages of its lifecycle (Byers and

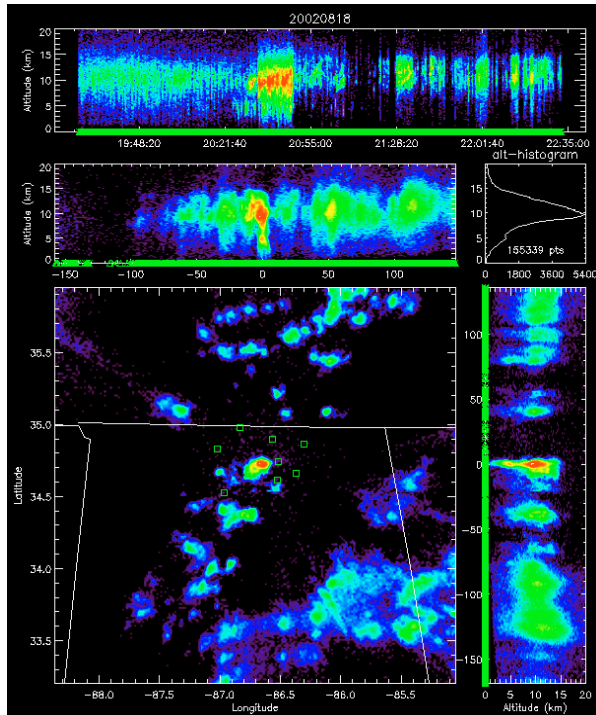


FIG. 6. LMA log density of sources for approximately 1935 – 2235 UTC on 18 August 2002. The XLMA program shows the LMA data in a 3-D image. The larger box on the bottom is a map of northern Alabama and part of southern Tennessee. The red contouring indicates areas where a high density of lightning sources was recorded over this time period. The small green boxes indicate LMA sensors. The NSSTC is located at the center of the network. This image clearly indicates that there was a maximum over the Huntsville area, with a smaller maximum just SSW of the HSV storm.

Braham, 1948).

Near the time of the microburst, the HSV storm was exhibiting a merger with a second storm located to its west; shortly following that, it merged one final time with a storm to its southwest (Fig. 7a). The first merger occurred immediately following the microburst occurrence. The process might have influenced the inflow to the storm, contributing to the onset of the microburst as the convergence of the storms and cloud dynamics influenced the vertical motion within the storm. The maximum reflectivity achieved at the surface was around 56 dBZ, occurring 12 minutes prior to and again 15 minutes after the microburst event at 2117 UTC. The storm reached a 60.8 dBZ peak reflectivity at a height of 7 km during the 2116–2121 UTC radar scan time. It reached its maximum vertical development of 17.5 km two scans later at 2126 UTC. At this time, the core of the HSV storm had merged with the second storm, as seen in Fig. 7a. Figure 7b shows the radial velocity during this timeframe. The divergence in the core of the storm is clearly visible at a height of 1.5 km. This is occurring along the southwest edge of the HSV storm near where it is beginning to show signs of a merger at this same height. [The HTX radar is to the northeast of this storm.] By 2126 UTC, a radial shear of  $30 \text{ m s}^{-1}$  occurs at the 1.5 km level. However, unlike at 2116 UTC where the value was

recorded in the storm's core, this is occurring to the south of where both storms have merged. This indicates that a strong inflow was present. In a later section, lightning rates for this event will be examined and there will be a strong indication that these lightning rates reflect the vertical motion within this storm.

#### 4.4 The Microburst Event

The microburst that occurred with the HSV storm produced torrential rainfall amounts as mentioned earlier. The surface reflectivity never dropped below 30 dBZ after 2029 UTC. The NSSTC recorded its daily high around the time of the microburst, indicating the air was quite warm at the surface. Fig. 8 shows the wind speeds recorded by the NSSTC anemometer. Several peaks can be seen in both the wind speed and peak wind plots, likely indicative of smaller downdrafts that preceded the microburst. The NSSTC was the only instrument in the area that recorded such high wind speeds along with the microburst gust, indicative of the small area over which the storm was concentrated.

The main mechanism for downdrafts is dependent on the melting of ice particles and evaporation of precipitation (Williams et al. 1999). As the water and ice particles in the upper portion of the cloud are evaporating and/or melting, this causes a gravitational loading effect; the mass of the cloud becomes heavier and falls to the ground. This effect was seen during the COoperative Huntsville Meteorological EXperiment (COHMEX) conducted during the summer of 1986 in Huntsville, Alabama (Goodman et al. 1988). It was observed during that study that, in fact, the primary mechanism that initiated microburst activity resulted from this evaporation and cooling of liquid and ice particles. The stronger the updraft and lifting of this liquid, the more intense the change of state. As these particles are moving vertically in such a way, charges are being interchanged between particles and the electrification process is initiated. In the next section, lightning rates will be compared to the onset of this microburst.

### 5. STORM ELECTRIFICATION

As mentioned in the previous section, the supercooled water acts as a growth agent for ice particles. As updrafts help modulate the supply of supercooled water, electrification is initiated due to the charge separations taking place (Williams et al. 1999). Therefore, lightning is dependent on this interaction. The more severe these updrafts, the more severe the system. Therefore, lightning rates can be indicative of strong vertical motion and storm severity.

#### 5.1 Flash Rates

The visual intensity of the lightning flashes during the HSV storm was later echoed by the impressive data sets that were examined. Previous studies (Goodman et al. 1988, Williams et al. 1989) have examined the onset times of IC and CG in relation to first IC vs. first

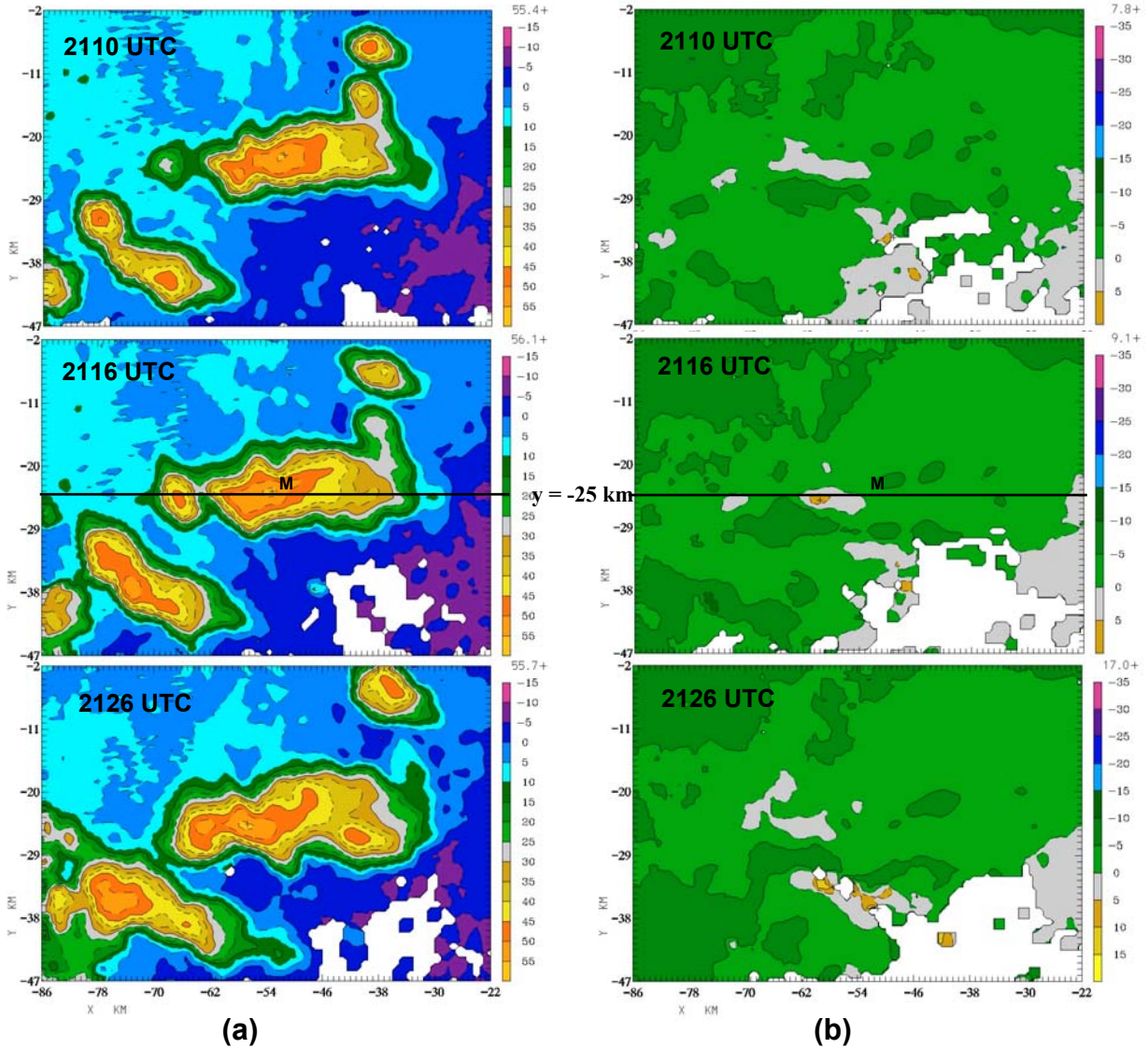


FIG. 7. (a) Reflectivity and (b) radial velocity images prior to, during, and after the microburst event of the HSV storm. The HSV storm is located in the center of the images. All reconstructed CAPPI images are shown at a height of  $z = 1.5$  km. The HSV storm produces a microburst at 2117 UTC. These images show that it was in the process of merging with a smaller cell moving east. As can be seen by the bottom two images, the storm began to merge with a larger storm and a strong area of divergence is seen occurring as an inflow to these storms. The line at  $y = -25$  km refers to the vertical cut through the storm's core as represented in Fig. 10. "M" denotes the location of the NSSTC where the microburst gust was recorded at 2117 UTC.

CG, as well as in relation to the severe weather events examined. However, the lightning for this storm was so intense it was difficult to break down these initial times. In comparison to the results of Williams et al. (1989), the observed peak rate of  $\geq 3$  total flashes per minute for that study was easily surpassed as the NLDN data for the HSV storm indicated a peak rate of  $> 8$  CG flashes per minute alone (Fig. 9). In contrast to the findings of Goodman et al. (1988), the peak total flash rate for the HSV microburst did not occur 4 minutes prior to the onset of the microburst. Instead, the peak rate occurred 10 minutes after the microburst and, before that, the previous maximum was at the time of the microburst (Fig. 9). Unlike these last two studies, though, the storm dynamics were different in that this storm was not

completely isolated during all the stages of its lifecycle.

The flash totals in Fig. 9 are a good representation of what the flash rates were for each radar scan. The times on the graph indicate the start time of each scan. As IC flashes accounted for 97.5% of all flashes, the LMA graph is a good indication of the IC trends as well as the overall trends. Sources were plotted as well to give an indication of their trends in relation to the overall flash totals. To make this feasible, the value of total sources was divided by 100 before being plotted. The NLDN data trends show that the occurrence of negative CG lightning dominated total CG rates, accounting for 78% of total CG flashes. Both the NLDN and LMA flash data indicate a jump in both IC and CG flash rates approximately 30-35 minutes before the microburst

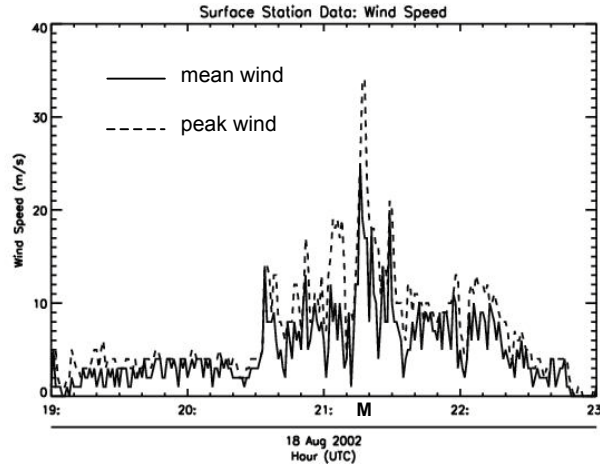


FIG. 8. One-minute mean and peak wind speeds as recorded by the NSSTC anemometer. The “M” represents the time of the microburst event at 2117 UTC. Several smaller peaks occur before the microburst as well as one more significant peak after the event. These represent smaller downdrafts as the storm is growing and the rain shaft is at its most intense. The peak after the microburst event may be due to a storm merger taking place around that timeframe.

onset. This is followed by a brief drop-off in flash rates before the rates increase again and reach their maxima. Notice that the first indications of values for both CG and total flashes occur for the scan time starting at 2023 UTC. Therefore, both IC and CG initiation took place at essentially the same time.

The flash rate trends also provide a good representation of the updraft strength of the storm. Williams et al. (1999) found that “jumps” in flash rates were an accompaniment of strong updraft surges. That study also saw a jump in IC flash rates as far in advance as fifteen minutes ahead of severe weather. In Fig. 10, the VIL content for the HSV storm is represented. As VIL values increase, so do the flash rates for both sets of lightning data. High VIL values imply large rates of charge separation. Therefore, cloud electrification intensifies and the lightning rates significantly increase.

The contoured Z and  $V_R$  images in Fig. 10 are vertical cuts at  $y = -25$  km (refer to Fig. 7) through the core of the HSV storm at the time of the microburst. A  $V_R$  value  $\geq 10$  m s<sup>-1</sup> is present at the surface. This inflow value is in line with where the Z contour plot shows the storms are beginning to join.

## 5.2 Flash Densities and Altitude

Fig. 11 shows two LMA log density maps of the north Alabama region. Unlike Fig. 6, the data set used to create these was more accurate and complete. However, there were too many events to combine in order to show the log density plot of the area during the time span of the HSV storm. In Fig. 6, there were a total of 105,000+ sources for an almost 2-hour timeframe whereas, now, there are over 200,000 sources just for these two 5-min plots alone.

An interesting feature of these plots is the altitude at which the source concentrations are located. In the

image for 2116 UTC, the highest density of the sources lies above the mixed phase region located at around 10 km. This is where a separation of charge between the negative and positive region of the cloud can be found. There is also a secondary maximum closer to the ground at 5 km. At 2126 UTC, the time of peak flash rate, there were two areas that saw a dense region of sources – just below the mixed phase and again just above it.

## 6. SUMMARY AND CONCLUSIONS

On 18 August 2002, storms earlier in the day left behind a boundary along which several strong storms formed along later in the afternoon, with a few becoming severe. As seen in Fig. 6, there were other areas that contained a high density of sources. However, none of these storms delivered the same lightning activity as the microburst-producing HSV storm. One storm that contributed to the second highest source density, as mentioned in Fig. 6, presented a higher surface reflectivity than the HSV storm and also contained hail. However, that storm’s max flash rate was 65.8 total

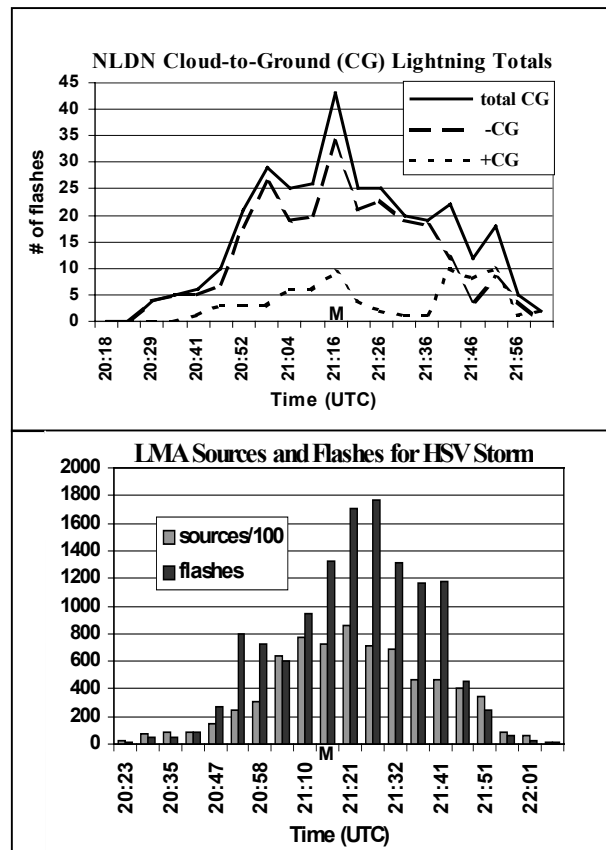


FIG. 9. Lightning flash rates for the HSV storm. The top graph provides CG lightning information as collected by the NLDN network; the bottom graph is based on LMA source data. The LMA data contains both IC and CG flashes. Two things are evident in these trends: 1) the peak in CG came before the peak in IC and 2) the amount of IC flashes clearly dominated. The “M” on each of the graphs denotes the time of the microburst event at 2117 UTC.

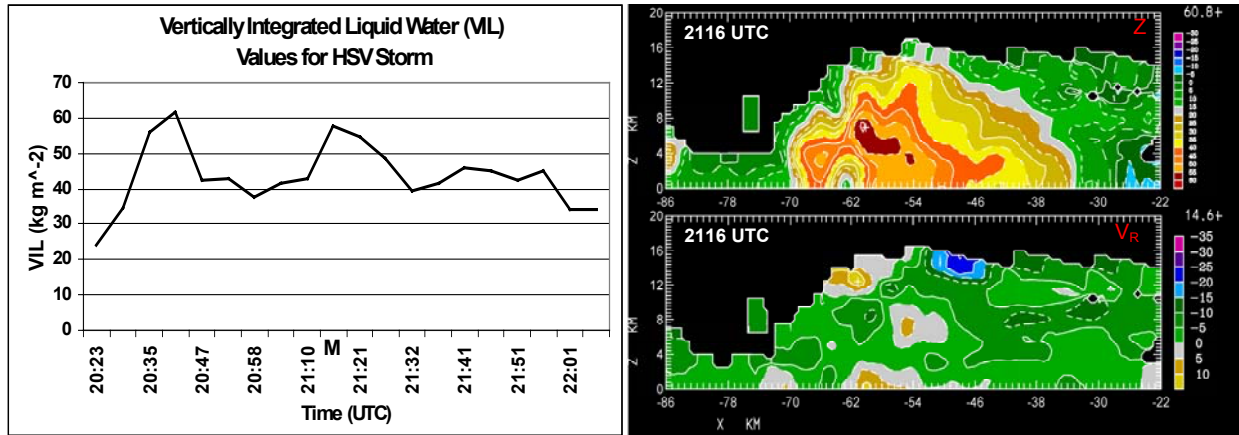


FIG. 10. The top image shows the VIL distribution during the lifetime of the HSV storm. The “M” indicates the time of the microburst at 2117 UTC. The color contour plots show vertical cuts of the storm through its core for the radar scan time of 2116 UTC at  $y = -25$  km (refer to Fig. 7) for  $Z$  and  $V_R$ . The max  $Z$  value is found at a height of 7 km just above where the max  $V_R$  is located at the ground.

flashes per minute, with an overall flash total of 2011 flashes – small in comparison to the HSV storm’s 12755 total flashes.

As the behavior of lightning in relation to updrafts, downdrafts, and the motion of supercooled water continue to be examined, the relation between these elements becomes more important. The HSV storm had an usually high flash rate and total amount of flashes for a non-supercell storm. The cloud physics and extreme vertical motion occurring within this microburst-producing storm likely contributed to the unusually high cloud electrification.

The values of the flash rates seemed directly related to VIL and updraft/downdraft motion. As in many case studies, IC flashes dominated, though a healthy amount of CG flashes – a rate of more than 8 per minute – also existed. More impressive was the total flash rate of 5.9 flashes per second achieved 10 minutes after the microburst event and possibly enhanced by a merger of cells.

Future work on this case includes a better understanding of the LMA algorithms and the NLDN flash retrieval systems. This was a highly irregular lightning event. Plotting the date in XLMA proved that

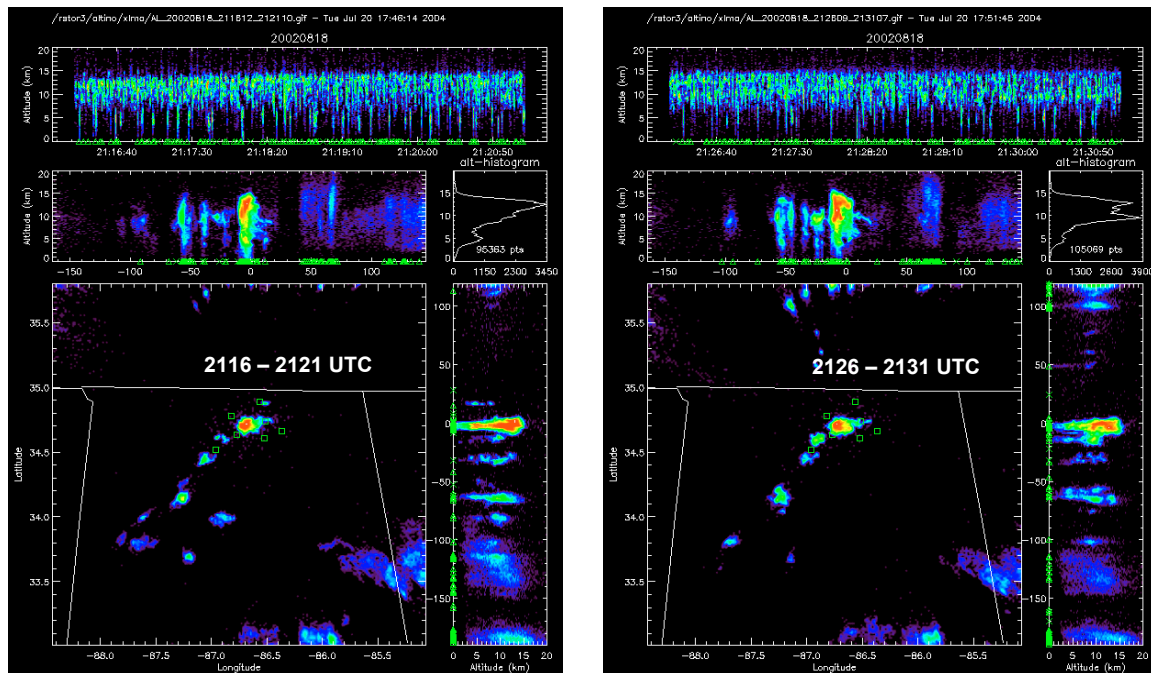


FIG. 11. LMA source density maps for the north Alabama region for 5-min periods beginning at 2116 UTC and 2126 UTC. Green triangles indicate NLDN flash data that was incorporated into the image. The concentration of these matches up with the high source densities for both images. Note the altitude(s) where the highest concentration of sources is at each time. For 2116 UTC, it is concentrated above the mixed-phase region while at 2126 UTC there is a peak above and below the 10 km threshold.

these rates were extreme and off the color scale. With this type of intensity, understanding how the flashes are broken down and interference resolved is of great importance.

This case study provides some insight as to how the liquid water content and vertical motion may or may not contribute to lightning enhancements. However, one of the more difficult aspects of this study was that this storm could not be examined individually as a single cell maturing through all the stages of development (Byers and Braham, 1948). At the same time, it is interesting to note that the two highest areas of source density in Fig. 6 are partially due to storm mergers. Though this study focuses on the relation of lightning directly to the microburst, these secondary characteristics prompt further interest and future study.

## REFERENCES

- Atkins, N. T., R.M. Wakimoto, 1991: Wet microburst activity over the southeastern United States: implications for forecasting. *Wea. Forecasting*, **6**, 470-482.
- Blakeslee, R., 2004: North Alabama Lightning Mapping Array (LMA) overview. *Proc. Total Lightning Applications, Transitions, Evaluation, Science and Technology (LATEST) Demonstration Workshop*, Huntsville, AL, NASA/MSFC.
- Byers, H. R., R. R. Braham, 1948: Thunderstorm structure and circulation. *J. Atmos. Sci.*, **5**, 71-86.
- Cummins, K. L., M. J. Murphy, E. A. Bardo, W. L. Hiscox, R. B. Pyle, and A. E. Pifer, 1998: A combined TOA/MDF technology upgrade of the U. S. National Lightning Detection Network. *J. Geophys. Res.*, **103**, 9035-9044.
- \_\_\_\_\_, M. J. Murphy, and J. V. Tuel, 2000: Lightning Detection Methods and Meteorological Applications. *IV Int. Symp. on Military Meteorology*, Malbork, Poland, September 25-28, 85-100.
- Goodman, S. J., D. E. Buechler, P. D. Wright, and W. D. Rust, 1988: Lightning and precipitation history of a microburst-producing storm. *Geophys. Res. Lett.*, **15**, 1185-1188.
- Greene, D. R., and R. A. Clark, 1972: Vertically integrated liquid water - a new analysis tool. *Mon. Wea. Rev.*, **100**, 548-552.
- Koshak, W. J., R. J. Solakiewicz, R. J. Blakeslee, S. J. Goodman, H. J. Christian, J. M. Hall, J. C. Bailey, E. P. Krider, M. G. Bateman, D. J. Boccippio, D. M. Mach, E. W. McCaul, M. F. Stewart, D. E. Buechler, W. A. Petersen, D. J. Cecil, 2004: North Alabama Lightning Mapping Array (LMA): VHF source retrieval algorithm and error analyses. *J. Atmos. Oceanic Technol.*, **21**, 543-558.
- Rison, B., 2004: Observations with the New Mexico Tech Lightning Mapping Array. *Proc. Total Lightning Applications, Transitions, Evaluation, Science and Technology (LATEST) Demonstration Workshop*, Huntsville, AL, NASA/MSFC, pp. 41.
- Thomas, R., P. Krehbiel, W. Rison, J. Hamlin, T. Harlin, N. Campbell, 2003: The LMA flash algorithm. *Proc. International Commission on Atmospheric Electricity (ICAE)*, Versailles, France, ICAE, pp. 2.
- Wakimoto, R. M., 1985: Forecasting dry microburst activity over the High Plains. *Mon. Wea. Rev.*, **113**, 1131-1143.
- Williams, E. R., 1998: The electrification of severe storms. *Severe Convective Storms, Severe Storms Monogr.*, No. 50, Amer. Meteor. Soc., 527-561.
- \_\_\_\_\_, B. Boldi, A. Matlin, M. Weber, S. Hodanish, D. Sharp, S. Goodman, R. Raghavan, and D. Buechler, 1999: The Behavior of Total Lightning Activity in Severe Florida Thunderstorms. *Special Issue of Atmos. Res.*, **51**, 245-265.